Supplementary Materials for

Glutamine blockade induces divergent metabolic programs to overcome tumor immune evasion

Robert D. Leone, Liang Zhao, Judson M. Englert, Im-Meng Sun, Min-Hee Oh, Im-Hong Sun, Matthew L. Arwood, Ian A. Bettencourt, Chirag H. Patel, Jiayu Wen, Ada Tam, Richard L. Blosser, Eva Prchalova, Jesse Alt, Rana Rais, Barbara S. Slusher, Jonathan D. Powell*

*Corresponding author. Email: poweljo@jhmi.edu

Published 7 November 2019 on *Science* First Release
DOI: 10.1126/science.aav2588

This PDF file includes:

Other Supporting Online Material for this manuscript includes the following:
(available at science.sciencemag.org/cgi/content/full/science.aav2588/DC1)

Materials and Methods

Mice

Six- to eight-week-old male or female mice were used for all experiments in this study. All mouse procedures were approved by the Johns Hopkins University Institutional Animal Care and Use Committee. C57BL/6, BALB/c, OTI, CD90.1 and $Rag2^{-/-}$ mice were initially obtained from The Jackson Laboratory. P14 transgenic mice were kindly provided by Dr. David A. Hildeman (Cincinnati Children's Hospital Medical Center).

Drugs

6-diazo-5-oxo-L-norleucine (DON) was purchased from Sigma-Aldrich (St. Louis, MO, USA). JHU083 (Ethyl 2-(2-Amino-4-methylpentanamido)-DON) was synthesized using previously described methods (*19, 25, 28*). CB839 was purchased from Cayman Chemical (Ann Arbor, Michigan).

Cell lines

MC38 cells were donated by CORVUS pharmaceuticals. B16-OVA melanoma cells were a gift from Hyam Levitsky. MC38OVA cells were a gift from Drew Pardoll (Johns Hopkins University). B16-F10, CT26, EL4, 4T1, 3LL (LL2) cell lines were obtained from the American Type Culture Collection (ATCC). The E)771 cell line was purchased from CH3 BioSystems. All cell lines were mycoplasma free via ELISA-based assays performed every 6 months. Unless otherwise noted, for in vitro assays, adherent cell cultures were incubated with 1 μM DON for 24 h before harvesting for analyses.

Flow cytometry, intracellular staining and cell sorting reagents

Antibodies against the following proteins were purchased from BD Biosciences: CD4 (RM4-5), CD69 (H1.2F3), CD90.1 (OX-7), CD122 (9TM-beta1), B220 (RA3-6B2), BCL-6 (K112-91), CD127 (M1/69), IFNg (XMG-1.2), TNFa (MP6-XT22), IL-2 (JES6-5H4). Abs against the following proteins were purchased from eBioscience: CD44 (IM7), CD11b (M1/70), CD11c (N418), EOMES (Dan11mag), Ki-67 (SolA15), KLRG1 (2F1), T-bet (eBio4B10). Abs against the following proteins were purchased from BioLegend: CD4 (RM4-5), CD27 (LG7F9), CD45 (30-F11), CD62L (MEL-14), CD137 (17-B5), PD-1 (29F.1A12) Bcl2 (BCL/10C4), and Granzyme B (GB11). Normal rabbit IgG (2729), anti-phospho-S6S240/244(5364), anti-TCF-1/7, anti-MCL-1, anti-H3K27Me3 (C36B11), anti-H3K4Me3 (C42D8), anti-H3K36Me3 (D5A7) were purchased from Cell Signaling Technology. Anti-VDAC1 (20B12AF2), anti-CPT1-alpha (8F6AE9), anti-TOMM20 (EPR15581-39) were purchased from Abcam. Anti-pimonidazole mouse IgG1 monoclonal antibody (MAb1) was purchased from Hypoxyprobe. Donkey anti-rabbit BV421 secondary Ab was purchased from BioLegend. Fc Block (2.4G2) and anti-CD28 (37.51) were purchased from BioXCell. Stimulatory anti-CD3 (2C11) was purified from hybridoma supernatants prepared in-house. Fixable viability dye eFluor780 was purchased from eBioscience; near IR fixable viability dye was purchased from Invitrogen. Flow cytometry experiments were performed on a FACS Celesta (BD Biosciences) and analyzed using FlowJo software (v.10.3; Tree Star). Cell sorting was performed on a FACSAria II or FACSAria Fusion (BD Biosciences). CD11b-CD11c-B220-CD45+TCRbeta+CD44+CD8+ TIL were isolated and collected in Trizol LS (Invitrogen) for RNAseq and RT-PCR experiments. Intracellular staining for cytokines was performed with BD Cytofix/Cytoperm fixation and/permeabilization solution (BD Biosciences). Intracellular staining for pimonidazole was performed with PFA (2%) fixation and 0.1% Triton X-100 permeabilization. All other intracellular staining was performed with eBioscience Foxp3 / Transcription Factor Staining Buffer Set (Invitrogen). Propidium iodide (ThermoFisher) staining was performed as per manufacturer's

recommendations. Flow cytometry data analyzed with Flowjo v. 10.0.7. Cell cycle analysis performed with Cell Cycle platform in Flowjo.

Western blot

Antibodies against the following proteins were purchased from Cell Signaling Technologies: ACSS2 (AceCS1) (#3658), c-Myc (#5605), phospho-AMPK (#2531), AMPK (#2532), CAD (11933), GMPS (14602), . Antibodies against the following proteins were purchased from Abcam: CTPS1 (ab133743), PFAS (ab186013), GFPT1 (ab125069). Antibody against ACSS2 (AceCS2) (17138-1-AP) was purchased from Proteintech. Antibody against pyruvate carboxylase (NBP1-4953655) was purchased from Novus. Antibody against GLS (701965) and PPAT (MA5-25926) were purchased from ThermoFisher. Antibody against ASNS (sc-365809) was purchased from Santa Cruz.

Tumor growth and survival experiments

Unless otherwise noted, all tumor injections were administered on the right flank. For the MC38 and MC38OVA, EL4 models, C57BL/6 wild type mice were injected with 5×10^5 tumor cells (s.c.) cultured in DMEM-based (MC38 and MC38OVA) or RPMI-based (EL4) media. 2×10^5 tumor cells (s.c.) were used in B16-F10 studies. For the CT26 model, BALB/c mice were injected with 5×10^5 CT26 cells (s.c.) cultured in RPMI-based media. JHU083 was dissolved in 2.5% ethanol in PBS (v/v) which was administered for all vehicle-treated control experiments. Groups were randomized based on tumor size on the day of beginning treatment. For MC38 and MC38OVA experiments, mice were treated with JHU083 or vehicle by daily gavage with 1 mg/kg/day in 100 µL for days 10-14 and with 0.3 mg/kg/day for day 15-24. For CD8 depletion studies, anti-mouse CD8β (clone 53-5.8), anti-mouse CD4 (clone GK1.5), and isotype

control (rat IgG1; clone HRPN) were administered (5 mg/kg) on the day before, the day after implantation, and weekly thereafter (*31*). For CT26 experiments, mice were treated with JHU083 or vehicle by daily gavage with 1 mg/kg/day in 100 uL for days 8-12 and with 0.3 mg/kg/day for day 13-22. For checkpoint experiments, anti-PD-1 mAb (RMP1-14, Bio X cell) was administered by i.p. injection (100 μg/mouse) for 4 doses on days 10, 12, 14, 16 (MC38 model), or days 8, 10, 12, 14 (CT26 model). For adoptive cellular therapy experiments in the OVA-expressing B16 melanoma model, C57BL/6 wild type mice received an injection of 2×10^5 B16-OVA melanoma cells (s.c.) cultured under OVA selection media containing 400 μg/ml G418 (Life technologies). Mice were treated with JHU083 or vehicle by daily gavage with 1 mg/kg/day in 100 uL for days 7-9 post tumor inoculation. Ten days after tumor injection, mice received an adoptive transfer of 1.5×10^6 activated OTI cells (r.o.), which had been stimulated *in vitro* with SIINFEKL peptide for 48 h, expanded in IL-2 (1 ng/mL) for 24 h and isolated with Ficoll-Paque Plus (GE Healthcare) gradient centrifugation. Mice were randomized based on tumor size before initiating anti-PD-1 therapy or transfer of activated OTI cells in the case of adoptive transfer experiments. Tumor burden was assessed every 2–4 days by measuring length and width of tumor. Tumor volume was calculated using the formula $V = (L \times W \times W)/2$, where V is tumor volume, W is tumor width and L is tumor length. Mice were sacrificed when tumor reached 2 cm in any dimension, became ulcerate or necrotic, or caused functional deficits. Unless otherwise specified, average tumor volume is depicted up until the time of first sacrifice.

TIL isolation

For TIL isolation experiments mice were treated with 0.3 mg/kg/day in 100 μL for days 14-18. Tumors were harvested from sacrificed mice on day 18 post tumor inoculation. Mice undergoing hypoxia staining received 80 mg/kg of Anti-pimonidazole mouse IgG1 monoclonal antibody (Hypoxyprobe) 90

minutes prior to tumor harvest. Explanted tumors were manually disrupted before incubating in collagenase type I (Gibco) and DNase (Roche) in RPMI for 30 min at 37 °C. Tumor mixtures, spleens and non-draining (left inguinal) and draining (right inguinal) lymph nodes were dissociated through a 70-µm filter and washed with PBS. Tumor suspensions were pelleted and resuspended in 40% Percoll solution which was underlaid with 80% Percoll in a 15 mL conical flask. After centrifugation at 2000 g for 30 min, the middle layer was removed, washed in PBS and counted. For *in vitro* stimulation assays, approximately $1x10^6$ cells per well in 96-well plate were stimulated in the presence of GolgiStop (BD Bioscience) for 4 h at 37 °C with either 10 µg/ml OVA class-I peptide (SIINFEKL) or PMA (50 ng/ml) and Ionomycin (500 ng/ml).

Histology

In some experiments, after tumor growth and pimonidazole pulsing (80 mg/kg i.p.), 90 minutes before harvesting), tumors were dissected, formalin fixed and sectioned. As per manufacturer's recommendations, warmed sections were de-waxed in xylene, rehydrated in stepwise decreasing concentrations of EtOH in water finally to 0.1% Tween 20 in Tris buffered saline. Tissue peroxidases were quenched with H_2O_2. Tissue was stained with hypoxyprobe-FITC conjugate and rabbit anti-FITC conjugated with horseradish peroxidase (Life Technologies), developed and counterstained with Gills #3 hematoxylin stain. Sections were imaged with an Olympus IX83 microscope.

Metabolomics and stable-isotope tracing

For tumor tissue experiments, a 20% (w/v) solution of [U-13C]Glucose in PBS was sterile-filtered and 100µl of this solution (i.e. 20 mg of [U-13C]Glc) was injected 3 times with 15-minute interval into the tail

vein of a restrained mouse without anesthesia. For 13C and 15N-glutamine tracing studies, 200uL of 0.2M solution were injected 3 times with 15-minute interval into the tail vein. Mice were killed via cervical dislocation at 45 min after first injection. Tumor tissue was rapidly harvested and frozen using a BioSqueezer (BioSpec Products) to quench metabolism and stored at -80°C prior to metabolite extraction. Metabolites were extracted from tissues weighing between 50-100mg in a methanol:water (80:20, v/v) extraction solution after homogenization with ultrasonic processor (UP200St, Hielscher Ultrasound Technology). Samples were vortexed and stored at -80°C for at least 2 hours to precipitate the proteins.

For *in vitro* T cell tracing experiments, isolated P14 T cells were activated (as described) in RPMI-based media with vehicle or DON (1uM) for 3 days. Activated T cells were counted in triplicate and brought up in tracing media with IL-2 and incubated for 6 hours at 37°C at $4x10^6$ cells per mL. Cells were transferred to Eppendorf tubes, washed with PBS, and centrifuged and flash frozen in liquid nitrogen. The day before analysis, cells were suspended in 80% MeOH, vortexed and incubated for at least 2 hours at -80°C to precipitate proteins. (For targeted metabolomics experiments, including quantitation of α-ketoglutarate levels, metabolite extraction was performed with acetonitrile/Methanol/H2O solution in a 2/2/1 ratio with 25μM phenylhydrazine to preserve α-keto acids). For *in vitro* MC38 cell tracing experiments, $1x10^6$ cells were plated on 10cm dishes in DMEM-based media for 24 hr, after which media was changed to media containing vehicle, DON (1 uM), or CB839 (1 uM) for an additional 24 hours. Media was tracing media for an additional 6h. Media was withdrawn from dishes, washed with PBS x2, and ice-cold 80% MeOH was added directly to plates. Cells were removed with cell scraper and transferred to Eppendorf tubes followed by flash freezing in liquid nitrogen. Samples were vortexed and stored at -80°C for at least 2 hours to precipitate the proteins. Tracer conditions include: Normal growth media with dialyzed FBS (10%) and [1,2-^{13}C]-acetate (100uM); Leucine-free growth media with dialyzed FBS and 1mM ^{13}C6-leucine; Glutamine-free growth media with dialyzed FBS (10%) and [13C-U]-

glutamine (4mM); Glucose-free growth media with dialyzed FBS (10%) and [13C-U]-glucose (25 mM for DMEM; 11mM for RPMI).

For all metabolomics and tracing experiments, supernatant was isolated after centrifugation at 15,000xg for 10min and dried under nitrogen gas and frozen at -80℃ for subsequent analysis by liquid-chromatography mass spectrometry (LC-MS). Dried metabolite extracts were resuspended in 50% acetonitrile solution. LC-MS based metabolomics profiling was performed on an Agilent LC-MS system. consisting of an Agilent 1290 Infinity Binary UHPLC pump and a 6230 time-of-flight mass spectrometer. Samples were analyzed in negative-ion mode. Chromatographic separations were performed using an Agilent 1290 ultra high performance liquid chromatography system with a wellplate autosampler (Agilent, Santa Clara, CA, USA). An ion pairing method was developed suing a C18 column (Agilent Zorbax Extend C18, 2.1 x 150 mm, 1.8 µm) with tributylamine as an ion- pairing agent, which enables the detection of most of the metabolites in central carbon metabolisms. The LC parameters were as follows: autosampler temperature, 4 ℃; injection volume, 2 µl; column temperature, 40 ℃; and flow rate, 0.25 ml/min. The solvents and optimized gradient conditions for LC were: Solvent A, 97% Water/3% methanol containing 5 mM TBA and 5.5 mM acetic acid; Solvent B, Methanol containing 5 mM TBA and 5.5 mM acetic acid; A non-linear gradient from 0% B to 99% B in 22 minutes with 5min of post-run time. A 6520 accurate-mass Q-TOF LC-MS system (Agilent) equipped with a dual electrospray (ESI) ion source was operated in negative-ion mode for metabolic profiling. The optimized ESI Q-TOF parameters for MS experiments were: ion polarity, negative; gas temperature, 325℃; drying gas, 10 L/min; nebulizer pressure, 45 psig; capillary voltage, 4000 V; fragmentor, 140 V; skimmer, 65 V; mass range, 50–1100 m/z; acquisition rate, 1.5 spectra/s; instrument state, extended dynamic range (1700 m/z, 2 GHz). Spectra were internally mass calibrated in real time by continuous infusion of a reference mass solution using an isocratic pump connected to a dual sprayer feeding into an electrospray ionization source. Data were acquired with MassHunter Acquisition software. A metabolite database with retention times based

on the ion-pairing method was developed using Agilent MassHunter PCDL manager software. The isotopologue peak extractions were achieved by Agilent MassHunter Profinder software. Relative metabolite abundance calculations were normalized per unit weight of tissue or, for *in vitro* MC38 experiments, per relative cell counts as determined by parallel cultures. T cell experiments were normalized across samples by cell counts.

In vitro T cell activation studies

Naïve P14 T cells were isolated with naïve CD8 negative selection cocktail and LS columns (Miltenyi) from splenocytes of P14 transgenic T cell mice. One million cells/mL in 12-well plate were activated with plate-bound anti-CD3 (5μg/mL) with soluble anti-CD28 (2μg/mL) and IL-2 (10ng/mL) in the presence of vehicle or DON (1uM) for 2 days. For FACS analysis of activation, memory and survival markers, cells were moved to non-coated plates and expanded with IL-2 (10 ng/mL) for 2 additional days with continued vehicle or DON. Cells were harvested, washed and analyzed by FACS. For restimulation experiments, including intracellular cytokine analysis by FACS, after the initial 2 days of activation, cells were moved to non-coated plates for 4 additional days, expanded on day 2 and day 4 with IL-2 (10 ng/mL) and continued vehicle or DON exposure. For restimulation, $1x10^6$ cells were washed and plated on a 96-well plate, precoated with anti-CD3 (1μg/mL) with soluble anti-CD28 (2μg/mL) for 4 h. Cells were washed and stained as described. For Seahorse metabolic flux analyses, isolated CD8+ T cells were activated for 3 days (as described above), washed and plated on Seahorse metabolic flux analysis plates, $1.5x10^5$ cells per well in a 96-well plate, and analyzed as described below.

LCMV-Armstrong infection

Two hundred fifty thousand naïve, CD90.1+ P14 T cells were adoptively transferred through retro-orbital injection into C57BL/6 mice that also received vaccination with LCMV-Armstrong virus ($2x10^5$ PFU) on the same day. Mice were treated on days 1-6 post infection with either vehicle or JHU083 (1 mg/kg/day); splenocytes were harvested on day 8 and analyzed by FACS. LCMV-Armstrong virus was originally obtained as a kind gift from Susan Kaech (Salk Institute for Biological Studies).

Metabolic Assays

P14 T cells activated in the presence of vehicle or DON as described above; for MC38 cells, $1x10^6$ cells were plated on 10cm dishes in DMEM-based media for 24 hr, after which media was changed to media containing vehicle, DON (1 uM), or CB839 (1 uM) for an additional 24 hours; cells were washed and trypsinized, counted and plated for seahorse analysis. Cells were plated on an XF96 cell culture microplate coated with poly-D lysine (50 μg/mL). Experiments were done in XF assay medium that contained 25 mM glucose, 2 mM L-glutamine and 1 mM Na pyruvate and analyzed using a Seahorse XF96 extracellular flux analyzer (Agilent Technologies). When indicated, the following were injected: oligomycin (1.5 μM), carbonyl cyanide 4-(trifluoromethoxy) phenylhydrazone (FCCP; 1.5 μM), rotenone (100 nM) and antimycin A (1 μM), BPTES (3 μM), etomoxir (4 μM), UK5099 (2 μM) (Sigma) . Basal ECAR, OCR and SRC reports were generated by Wave Desktop software (Agilent Technologies).

Measurement of cellular NADPH/NADP+ ratio

Total cellular NADPH/NADP+ ratio were determined by an NADPH/NADP-Glo assay kit (Promega, Wisconsin, USA) per manufacturer's instructions.

Measurement of glucose-6-phosphate dehydrogenase activity

Performed by Glucose-6-Phosphate Dehydrogenase (G6PD) Activity Assay Kit (Cell signaling #12581) performed according to manufacturer's instructions. Protein was quantified using BCA kit per manufacturer's protocol (Sigma)

RNA Sequencing and Analysis

CD11b-CD11c-B220-CD45+TCRbeta+CD44+CD8+ TIL from vehicle or JHU083 treated MC38 tumor-bearing mice were sorted on BD FACSAria Fusion and collected in Trizol LS (Invitrogen) as described. Samples were sent to Admera Health for RNA extraction, library construction and sequencing. Total RNA from 5 individual mice (not pooled) in each treatment group was isolated. Paramagnetic beads coupled with oligo d(T) were combined with total RNA to isolate poly(A)$^+$ transcripts based on NEBNext Poly(A) mRNA Magnetic Isolation Module manual. Prior to first strand synthesis, samples were randomly primed (5´ d(N6) 3´ [N=A,C,G,T]) and fragmented based on manufacturer's recommendation (NEBNext Ultra Directional RNA Library Prep Kit for Illumina). The first strand was synthesized with the Protoscript II Reverse Transcriptase with a longer extension period (40 minutes for 42°C). All remaining steps for library construction were used according to the NEBNext Ultra Directional RNA Library Prep Kit for Illumina. Illumina 8-nt dual-indices were used. Samples were sequenced on a HiSeq with a read length configuration of 1x75bp.

The transcriptomic analysis work flow began with a thorough quality check by FastQC v0.10.1 and quality thresholding of the raw sequencing reads. The major stages of analysis included read mapping to the latest reference genome (GRCM38), assembly of the mapped reads to identify expressed transcripts and genes, followed by quantification and comparison of the assembled transcriptomes between cells. Gene and transcript expression between the comparing RNASeq samples were quantified and reported

as FPKM (Fragments Per Kilobase of transcript per Million mapped reads) units, followed by visualization and exploration of results. We employed GSEA in the context of gene ontology. To perform GSEA, we utilized gene sets available on the BROAD website (http://www.broadinstitute.org/gsea/). Specific gene sets used include: GSE10239_MEMORY_VS_KLRG1HIGH_EFF_CD8_TCELL_UP (Fig. 3H), HALLMARK_HYPOXIA (Fig. 3E), REACTOME_APOPTOSIS (Fig. 3J), POSITIVE_REGULATION_OF_ALPH_BETA_T_CELL_PROLIFERATION (Fig. 3B), POSITIVE_REGULATION_OF_ALPH_BETA_T_CELL_ACTIVATION (Fig. 3C), SAFFORD_T_LYMPHOCYTE_ANERGY (Fig. S3C, right), GSE9650_EXHAUSTED_VS_MEMORY_CD8_TCELL_UP (Fig. S3C, left), GO_CELLULAR_RESPONSE_TO_OXIDATIVE_STRESS (Fig. S3G). Enrichment scores (ES), p-values and false discovery rates are denoted within the figures, with an FDR cutoff of $\leq$0.25 considered significant for hypothesis generation.

Real-time PCR analysis

CD8+ TIL were sorted as described. Total RNA was isolated from TRIzol LS reagent (Invitrogen) following the manufacturer's protocol. RNA (800 ng) was then reverse transcribed to cDNA with ProtoScript II Reverse Transcriptase (New England BioLabs). Real-time PCR was performed using EagleTaq Universal Master Mix (Roche). Real-time PCR primers and probes were obtained from Applied Biosystems: BCL2 Related Ovarian Killer (*Bok; Mm00479422_m1*); Caspase 12 (*Casp12; Mm00438038_m1*); BCL2 Interacting Protein 3 (*Bnip3;Mm01275600_g1*); TNF Receptor Superfamily Member 10b (*Tnfrsf10b; Mm00457866_m1*); Fas Cell Surface Death Receptor (*Fas;Mm01204974_m1*); B Cell Receptor Associated Protein 31 (*Bcap31;Mm00478914_m1*); Caspase 7 (*Casp7;Mm00432322_m1*); Caspase 8 (*Casp8;Mm01255716_m1*); *(Nadsyn1; Mm00513448_m1)* . Values of ΔΔ cycle threshold were

normalized to the housekeeping gene 18s rRNA (Life Technologies) and further normalized to the control group. Experiments were performed on an OneStepPlus 96-well instrument (Applied Biosystems).

Stable knockdown cell line generation

TRC lentiviral shRNAs targeting *Asns, Cad, Ctps1, Gfpt1,Gls, Gmps1, Nadsyn1, Pfas,* and *Ppat* were obtained from Sigma. The TRC number for each shRNA is as follows:

Gene ID	Gene Symbol	Clone ID		Gene ID	Gene Symbol	Clone ID
14583	Gfpt1 shRNA-1	TRCN0000031644		14660	Gls	TRCN0000051137
14583	Gfpt1 shRNA-2	TRCN0000031646				
14583	Gfpt1 shRNA-3	TRCN0000031648		27053	Asns shRNA-1	TRCN0000031699
				27053	Asns shRNA-2	TRCN0000031701
229363	Gmps shRNA-1	TRCN0000045938		27053	Asns shRNA-3	TRCN0000031702
231327	Ppat shRNA-1	TRCN0000031618		237823	Pfas shRNA-1	TRCN0000341134
231327	Ppat shRNA-2	TRCN0000031614		237823	Pfas shRNA-2	TRCN0000341135
231327	Ppat shRNA-3	TRCN0000031615		237823	Pfas shRNA-3	TRCN0000341062
51797	Ctps shRNA-1	TRCN0000032546		78914	Nadsyn1 shRNA-1	TRCN0000112435
51797	Ctps shRNA-2	TRCN0000032544		78914	Nadsyn1 shRNA-2	TRCN0000112437
51797	Ctps shRNA-3	TRCN0000032545		78914	Nadsyn1 shRNA-3	TRCN0000112439
231327	Ppat shRNA-1	TRCN0000031618		69719	Cad shRNA-1	TRCN0000032550
231327	Ppat shRNA-2	TRCN0000031614		69719	Cad shRNA-2	TRCN0000032551
231327	Ppat shRNA-3	TRCN0000031615				

Lentivirus production and cell transduction

HEK293T cells were seeded in 6-well plates. Cells were co-transfected with 1.6 μg lentiviral vector (empty vector or shRNA targeting indicated proteins) + 1.2 μg pspAX2 + 0.4 μg pMD2G using Lipofectamine 3000 (Thermo Fisher) according to manufacturer's instructions. Media was changed after 24 hr and at 48 hr and 72 hr, the supernatants were harvested and stored at −80°C.

MC38 cells were seeded in 6-well culture plates. When cells were 40-50% confluent, lentiviral supernatants were added to culture medium. After 24 hr, cells were treated with puromycin (2ug/mL) to select transduced cells.

Cell proliferation assays

For adherent cultures, $2.5x10^3$ cancer cells were plated in each well of a 96-well plate and allowed to attach for 24 h. At 24 h additional media was added containing DON to allow final concentrations as noted. Cells were incubated for an additional 48-72 h at 37°C. After 48-72 h cells were quantitated with CyQUANT cell proliferation assay (Invitrogen) as per manufacturer's directions.

Statistics

All graphs were created using GraphPad Prism software and statistical analyses were calculated using GraphPad Prism. Comparisons between two independent groups were assessed by two-tail Student's t test or one-way ANOVA with Sidak correction for multiple groups comparison μM). Log-rank (Mantel-Cox) tests were performed for survival data. Tumor growth curves were assessed by two-way ANOVA

with Sidak correction for multiple comparisons as recommended by GraphPad statistical program. A *p* value of less than 0.05 was considered statistically significant. Principal component analysis was performed with JMP statistical software v.13 (SAS).

Data S1

RNAseq expression data comparing CD11b-CD11c-B220-CD45+TCRbeta+CD44+CD8+ TIL from MC38 tumor bearing mice treated with vehicle or JHU083.

Supplementary Figure Legends

Fig. S1 Glutamine blockade suppresses cancer cell proliferation, viability and cell cycle progression. (**A-C**) Cell proliferation assay of MC38 (A), CT26 (B) and EL4 (C) tumor cells treated with increasing concentrations of DON for 48h. (**D)** Cell viability assay of MC38 cells treated with increasing concentrations of DON for 24 hours. (**E**) Cell cycle analysis of MC38 cells incubated with 1uM DON for 24 hours. Data are representative of three independent experiments (A-C, E) with 3-4 technical replicates per data point. Statistics for cell cycle data were assessed with two-tailed student's t-test for multiple comparisons. ns, not significant; *p < 0.05, **p < 0.01, ***p < 0.001.

Fig. S2 DON prodrug JHU083 demonstrates *in vivo* antitumor efficacy in multiple tumor models. (**A**) Chemical structures of L-glutamine, DON, and JHU083. (**B**) ^{1}H NMR data for JHU083, compound 4a in *(25)*. (**C**) Pharmacokinetic analysis of JHU083 in the MC38 tumor model demonstrating tumor site enrichment over plasma. Of note, due to higher levels of circulating enzymes in mice and other rodents, the prodrug is much more rapidly converted to active drug (DON) in these species when compared with larger animals. Thus, while rodents are not ideal hosts to evaluate pharmacokinetics for these compounds, we demonstrate the establishment of a robust therapeutic window. (**D-F)** Tumor growth curve (left) and survival curve (right) from vehicle and JHU083 treated CT26 (D), B16 (E), and EL4 (F)

tumor-bearing mice. (**G**) Global metabolite pool sizes from explanted vehicle and JHU083-treated MC38 tumors. (**H**) CT26 bearing BALB/c mice treated with vehicle, JHU083, anti-PD-1, or combination JHU083 and anti-PD-1 beginning on day 8 after tumor inoculation. Tumor growth curve (left) and survival curve (right) are shown. Error bars represent SEM. Log-rank (Mantel-Cox) tests were performed for survival data. Tumor growth curves were assessed by two-way ANOVA with Sidak correction. Data are representative of three independent experiments with n = 5-10 per group. **p < 0.01, ****p < 0.0001.

Fig. S3 Glutamine blockade conditions CD8+ TIL towards a highly proliferative, activated and long-lived phenotype

(**A-C, F-H**) C57BL/6 mice with MC38 OR MC38OVA tumors were treated with vehicle or JHU083 (0.3 mg/kg/day) on days 14-18. Tumors were harvested on day 18 and CD44+CD8+ TIL were sorted for RNAseq analysis (**C, G-I**) or RT-PCR (**L**). Volcano plots showing changes in gene expression in CD44+CD8+ TIL from vehicle treated vs JHU083 treated MC38-bearing mice (A-B). (C) GSEA tracings for exhausted vs memory CD8 phenotype (left) and T lymphocyte anergy (right). (**D-E, I-J**) C57BL/6 mice with MC38 tumors were treated with vehicle, anti-PD-1 (200μg/mouse on days 14 and 16), JHU083 (0.3 mg/kg/day on days 14-18), or combination JHU083 (0.3 mg/kg/day on days 14-18) and anti-PD-1 (200μg/mouse on days 14,16). FACS summary data for MFI of CD44 (D), percentage PD-1+LAG-3+ double positive CD8+ TIL (E). (**F**) FACS plots and data summary showing percentage IL-2+ cells per TetOVA+CD8+ from MC38OVA model after *ex vivo* stim. (**G**) GSEA tracing for oxidative stress. (**H-I**) GSEA tracing (H) and heat map (I) of leading edge genes driving apoptotic pathways in CD44+CD8+ TIL. FACS summary data for MFI of CD62L (J), CD122 (K) for CD8+ TIL. (**L**) Relative mRNA expression levels of apoptotic gene from CD8+ TIL by RT-PCR. (**M-O**) $2.5x10^5$ naïve CD90.1+ P14 T cells were adoptively transferred into C57BL/6 mice that received vaccination with LCMV-Armstrong virus. Mice were treated on days 1-6 post infection with

vehicle or JHU083 (1 mg/kg/day); splenocytes were harvested on day 8 and analyzed with GP33-tetramer staining by FACS. Summary data is shown for activation markers (A), memory markers (B) and survival markers (C). Error bars represent SEM. For MC38 experiments FACS summary plots are combination data from 2 independent experiments with n = 5 mice per group. RNA-seq data are from treated and untreated groups of 5 mice in each group. For LCMV viral challenge experiments data are representative from 3 independent experiments with n = 4 mice per group. *$p < 0.05$, **$p < 0.01$, ***$p < 0.001$ using two-tailed Student's t test for multiple groups comparison or two-tailed Student's t test.

Fig. S4 Activated CD8+ T cells and cancer cells display distinct metabolic phenotypes in response to glutamine antagonism. (**A-B**) ECAR (left) and OCR (right) trace of CT26 (A) and B16-F10 (B) tumor cells pretreated for 24 h with vehicle or DON (5 μM). (**C**) Data summaries from metabolic flux analysis from P14 T cells activated for 3 days as described in the presence or absence of DON (1 μM). (**D**) LCMS analysis of TCA intermediates after stable isotope tracing with [$^{13}C_6$]-L-leucine. (**E**) Transcript levels for ACSS1 (left) and ACSS2 (right) from RNA seq data set. (**F**) Western blot analysis of ACSS1, ACSS2 and c-MYC expression in murine cancer cell lines +/- DON as noted. Error bars represent SEM. *$p < 0.05$, **$p < 0.01$, ***$p < 0.001$, ****$p < 0.0001$ using two-tailed Student's t test.

Fig. S5 Suppression of glutamine requiring metabolic pathways by glutamine antagonists. LCMS analysis of TCA intermediates after stable isotope tracing with [U-13N] glutamine (top and center rows) and [U-13C] glutamine (bottom row) for *in vitro* DON-treated MC38 cells (first column), JHU083-treated *in vivo* MC38 tumors (center column) and *in vitro* DON-treated activated P14 T cells (last column). Error

bars represent SEM. *p < 0.05, **p < 0.01, ***p < 0.001, ****p < 0.0001 using two-tailed Student's t test for multiple groups comparison or two-tailed Student's t test.

Fig. S6 Comparison of metabolic adaptations of MC38 cells treated with glutamine antagonism vs targeted glutaminase inhibition. (**A-G**) MC38 cells treated for 24 hours with Vehicle, DON, or CB839 before 6-hour tracing incubation. LCMS analysis of TCA intermediates after stable isotope tracing with [U-13C] glucose (A). Relative [U-13C] glucose labeling of TCA isotopologues characteristic of pyruvate carboxylase (PC) activity (B). Western blot analysis of pyruvate carboxylase (PC) and c-MYC expression in vehicle, DON, or CB839 treated MC38 cells, and vehicle or DON-treated activated P14 T cells (C). 2-NBDG uptake by FACS (D). Western blot analysis of phospho-AMP kinase (p-AMPK) and total AMPK in vehicle, DON, or CB839 treated MC38 cells (E). Relative AMP/ATP ratio from LCMS (F). Relative NADPH/NADP+ ratio (G). Error bars represent SEM. *p < 0.05, **p < 0.01, ***p < 0.001, ****p < 0.0001 using two-tailed Student's t test for multiple groups comparison.

Fig. S7 Targeted inhibition of glutamine dependent pathways partially contributes to the metabolic phenotype of DON-treated MC38 cells. (**A**) Glutamine requiring enzymes targeted for shRNA knockdown in the MC38 cell line are shown. (**B**) Western blots showing knockdown efficiency in MC38 cells using multiple constructs (constructs selected for data presentation shown in red). (**C**) RT-PCR showing transcript knockdown for *Nadsyn1*. (**D**) Western blot analysis for c-MYC in wild type and shRNA-Lentivirus transfected MC38 cells with and without DON treatment for 24 hours (EV; Empty Vector); densitometry for c-MYC shown below blot, DON-treated in red; blot representative of 4-5 independent experiments. (**E**) 2-NBDG uptake by flow cytometry analysis for shRNA-Lentivirus transfected MC38 cells; data is combined and normalized from 2 independent experiments. (**F**) Cell proliferation assay of shRNA-

Lentivirus transfected MC38 cells at 96 hours; data is combined and normalized from 2 independent experiments. (**G**) Principal component analysis of shRNA-Lentivirus transfected MC38 using data from (D-F) for c-MYC expression, 2-NBDG uptake, and CyQuant proliferation assay. Error bars represent SEM. *$p < 0.05$, **$p < 0.01$, ***$p < 0.001$, ****$p < 0.0001$ using one-way ANOVA statistical analyses.

Supplemental Figure 1

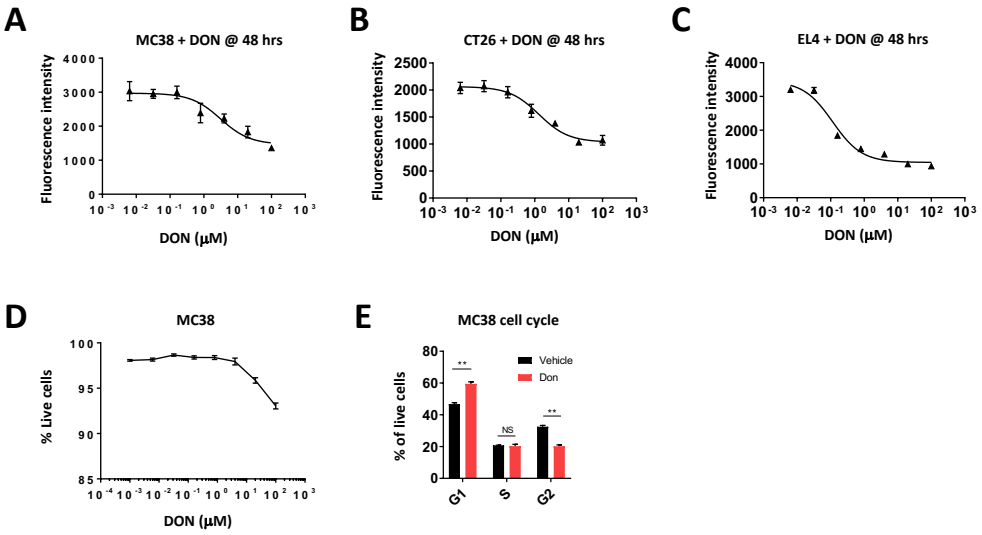

Supplemental Figure 2

A

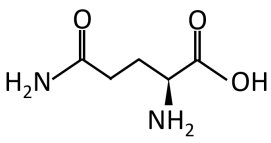

L-Glutamine

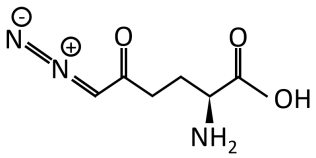

6-Diazo-5-oxo-L-norleucine (DON)

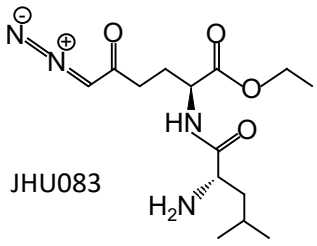

JHU083

B **Ethyl (S)-2-((S)-2-Amino-4-methylpentanamido)-6-diazo-5-oxohexanoate**: 1H NMR (CDCl3): δ 0.94 (d, J = 6.4 Hz, 3H), 0.97 (d, J = 6.4 Hz, 3H), 1.27 (3H, t, J = 7.1), 1.28–1.37 (1H, m), 1.45 (2H, s), 1.57–1.83 (2H, m), 1.92–2.08 (1H, m), 2.16–2.26 (1H, m), 2.26–2.49 (2H, m), 3.39 (1H, dd, J = 10.0, 3.9), 4.19 (2H, dq, J = 7.1, 1.4), 4.54 (1H, dt, J = 8.5, 4.8), 5.30 (1H, s), 7.85 (1H, d, J = 8.3). 13C NMR (CDCl3): 14.25, 21.40, 23.54, 24.97, 27.71, 36.82, 44.29, 51.48, 53.60, 54.86, 61.65, 171.99, 175.99, 193.67.
Optical rotation: [α]22D + 13° (c 0.323, CHCl3)

C

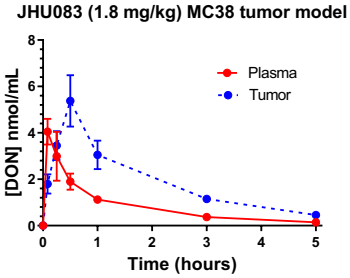

	JHU-083			
PK parameters	C_{max} (nmol/mL)	T_{max} (h)	AUC_{last} (h.nmol/mL)	Tumor/plasma
Plasma	4.1±0.24	0.083	4.1	~
Tumor	5.38±0.73	0.5	9.5	2.31

D

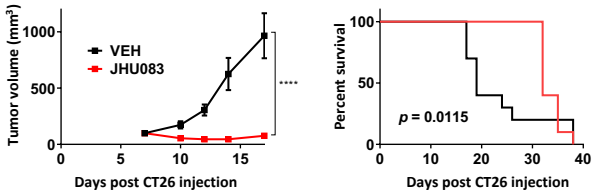

E

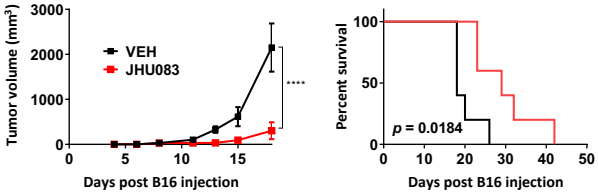

F

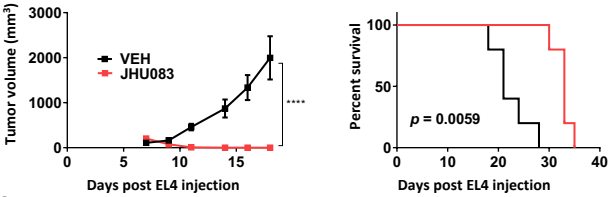

G

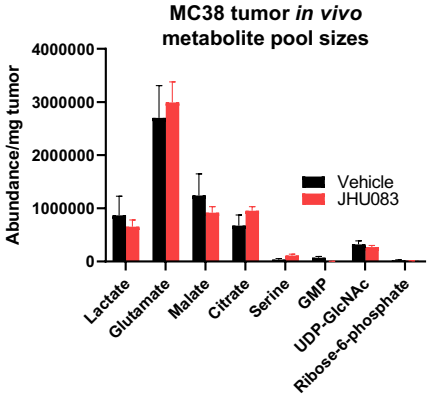

H

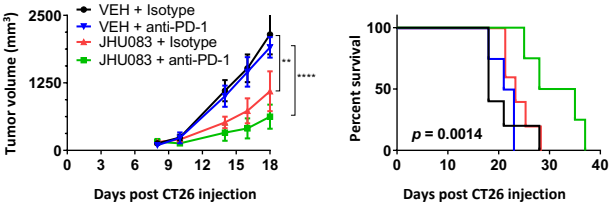

Supplemental Figure 3

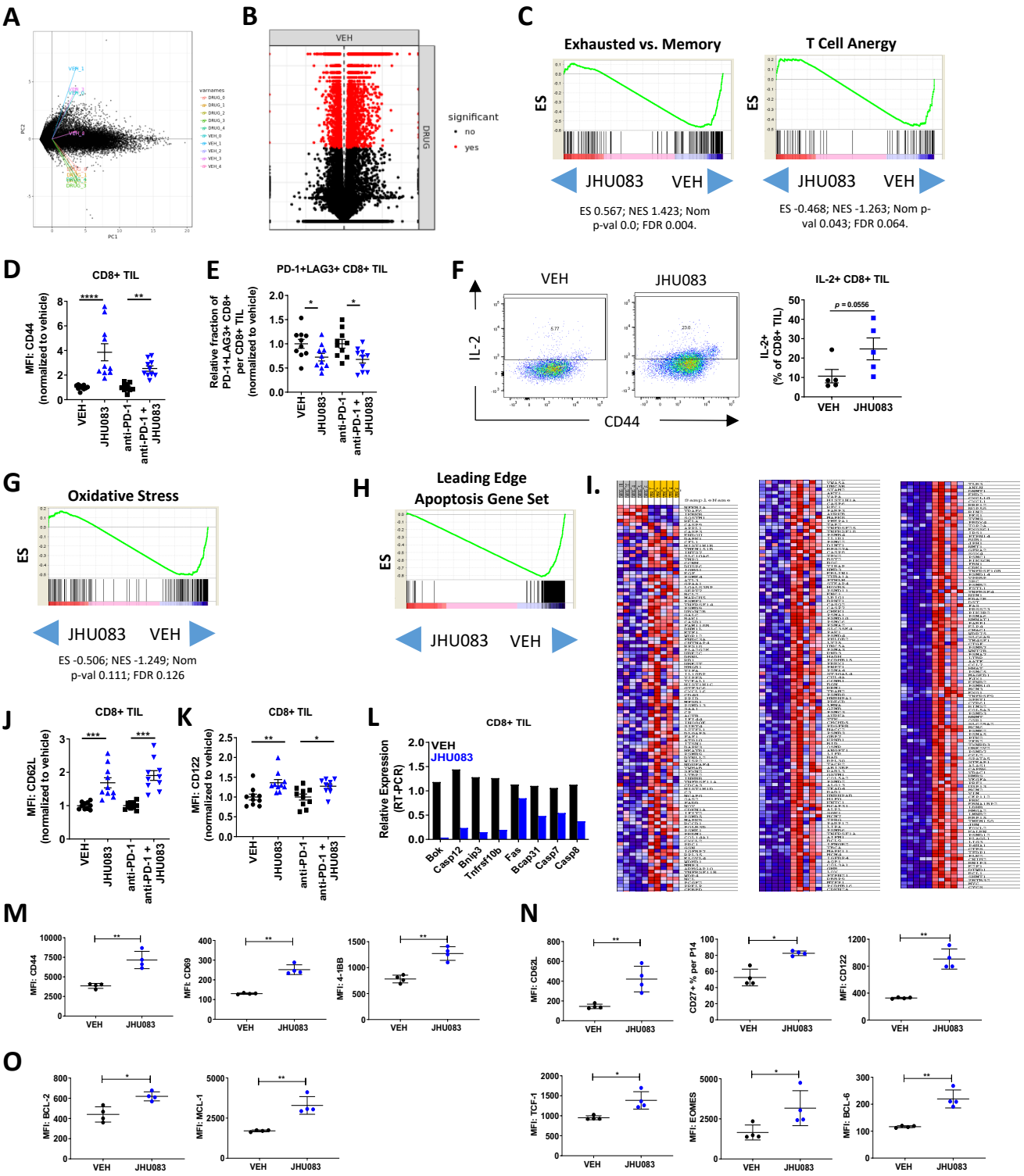

Supplemental Figure 4

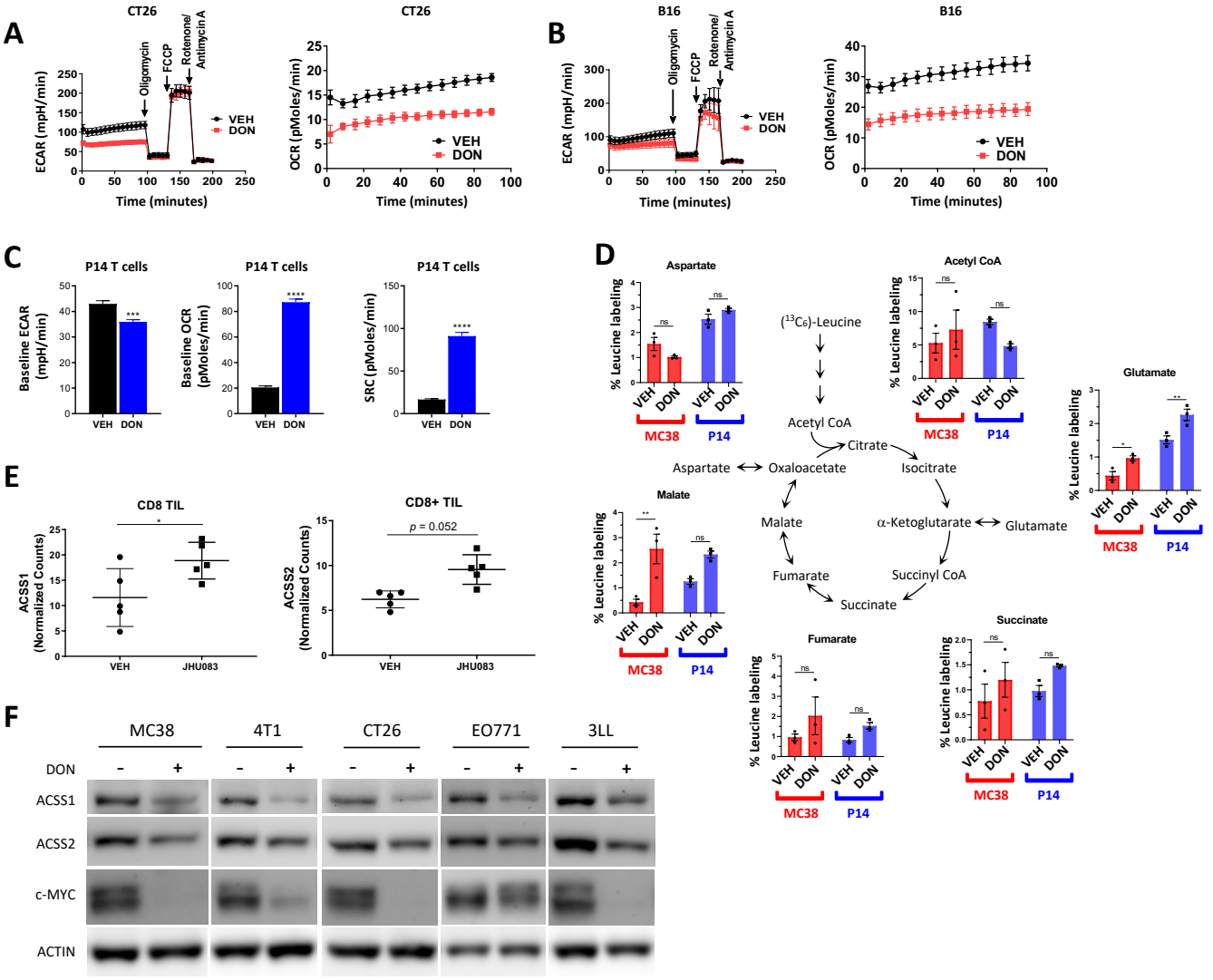

Supplemental Figure 5

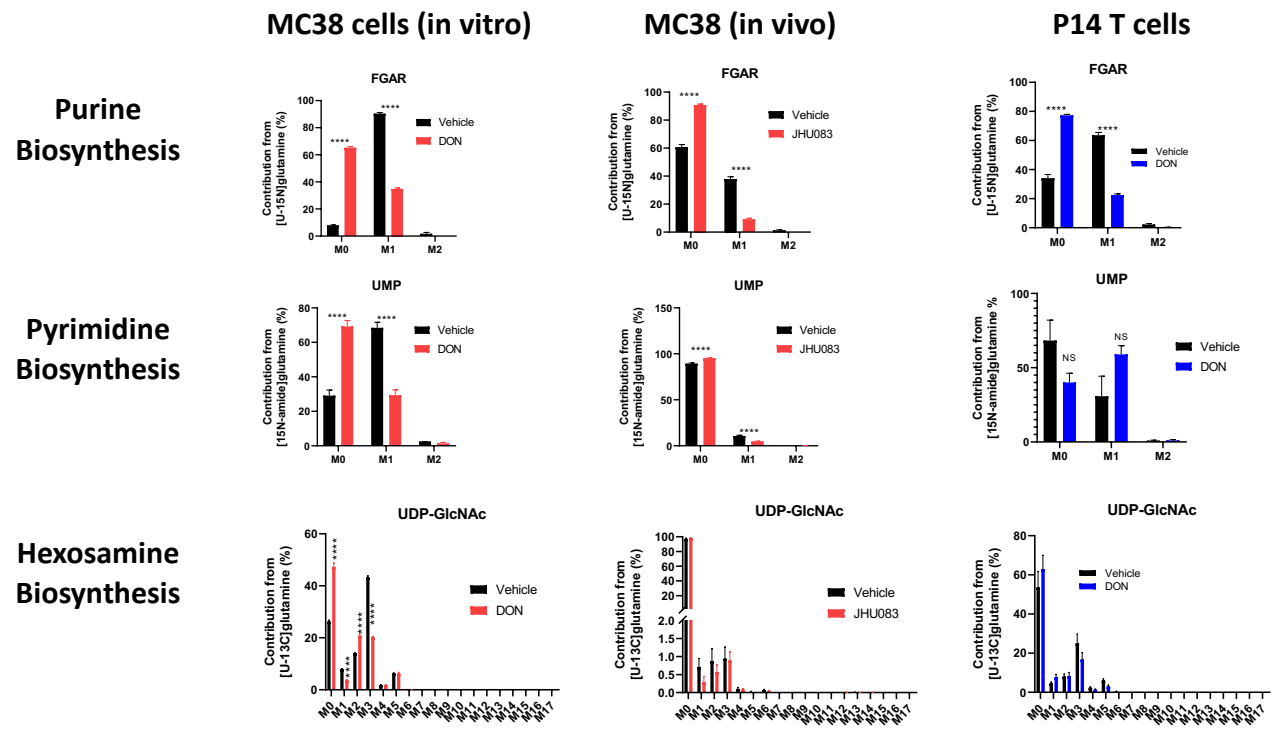

Supplemental Figure 6

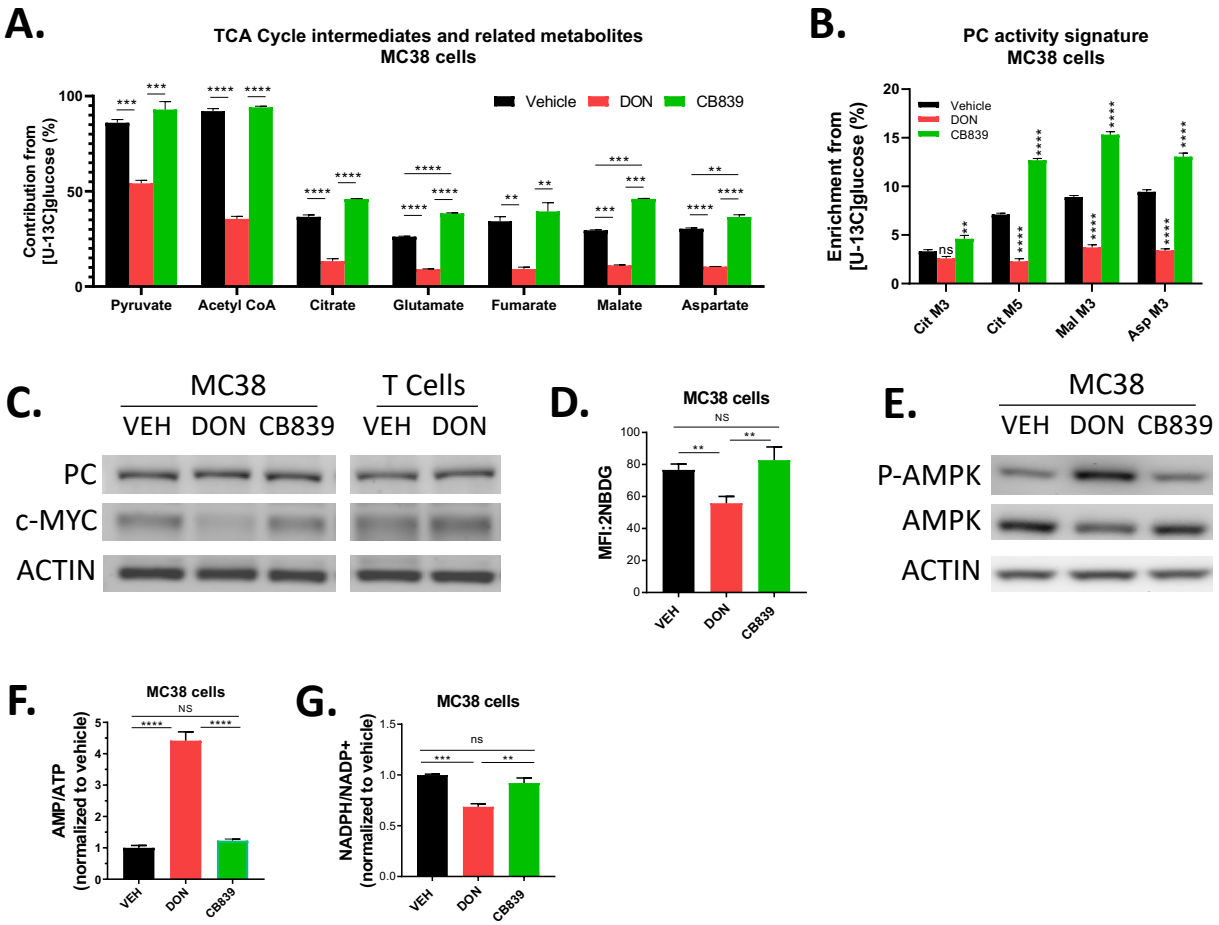

Supplemental Figure 7

A.

Pathway	Enzyme Targeted for Knockdown
Nucleotide synthesis	Phosphoribosyl Pyrophosphate Amidotransferase (PPAT)
Purine synthesis	Phosphoribosylformylglycinamidine Synthase (PFAS)
Purine synthesis	Guanine Monophosphate Synthase (GMPS)
Pyrimidine synthesis	Carbamoyl-Phosphate Synthetase (CAD)
Pyrimidine synthesis	CTP Synthase 1 (CTPS1)
Coenzyme synthesis	NAD+ Synthetase 1 (NADSYN1)
Glutaminolysis	Glutaminase (GLS)
Amino acid synthesis	Asparagine Synthetase (ASNS)
Hexosamine synthesis	Glutamine--Fructose-6-Phosphate Transaminase 1 (GFPT1)

B.

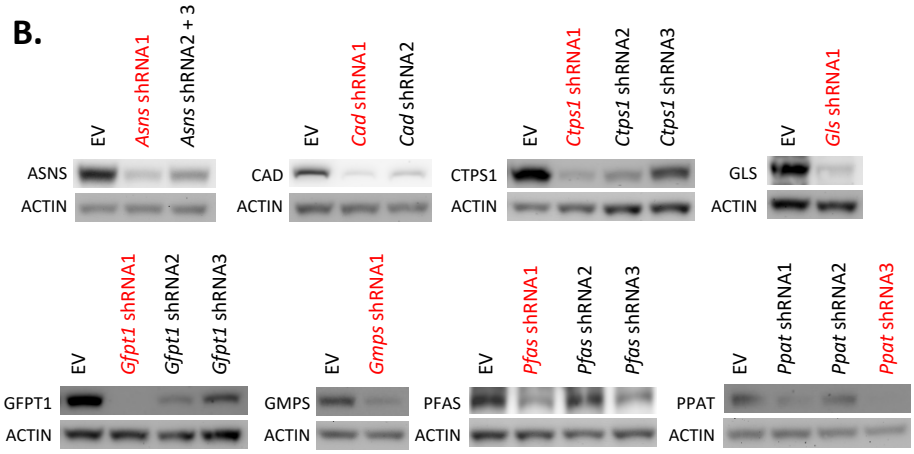

C.

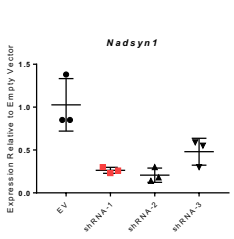

D.

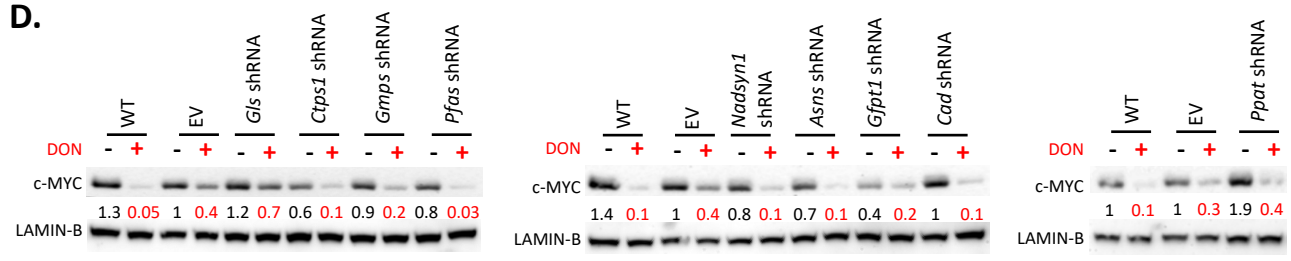

E.

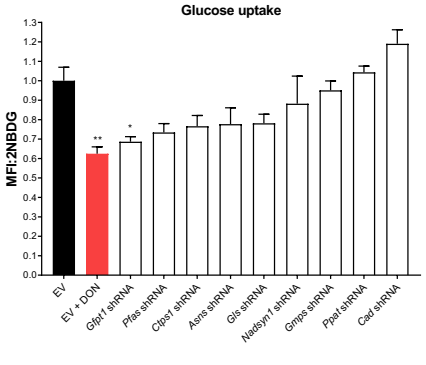

F.

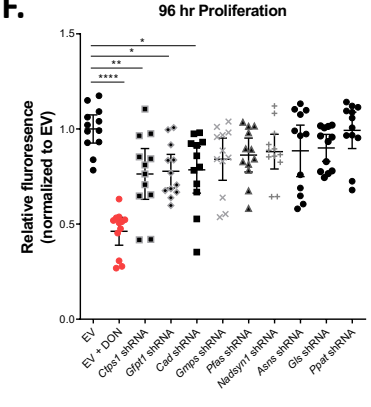

G.

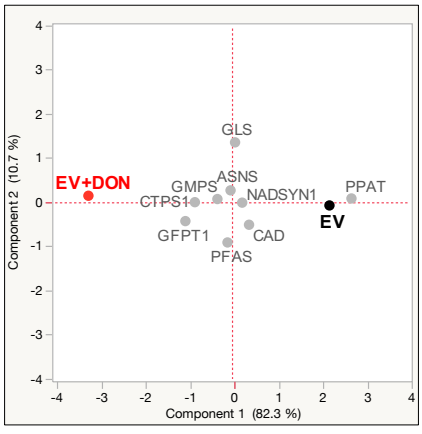

References and Notes

1. N. N. Pavlova, C. B. Thompson, The emerging hallmarks of cancer metabolism. *Cell Metab.* **23**, 27–47 (2016). doi:10.1016/j.cmet.2015.12.006 Medline

2. A. J. Wolpaw, C. V. Dang, Exploiting metabolic vulnerabilities of cancer with precision and accuracy. *Trends Cell Biol.* **28**, 201–212 (2018). doi:10.1016/j.tcb.2017.11.006 Medline

3. B. J. Altman, Z. E. Stine, C. V. Dang, From Krebs to clinic: Glutamine metabolism to cancer therapy. *Nat. Rev. Cancer* **16**, 619–634 (2016). doi:10.1038/nrc.2016.71 Medline

4. J. Zhang, N. N. Pavlova, C. B. Thompson, Cancer cell metabolism: The essential role of the nonessential amino acid, glutamine. *EMBO J.* **36**, 1302–1315 (2017). doi:10.15252/embj.201696151 Medline

5. K. A. Frauwirth, J. L. Riley, M. H. Harris, R. V. Parry, J. C. Rathmell, D. R. Plas, R. L. Elstrom, C. H. June, C. B. Thompson, The CD28 signaling pathway regulates glucose metabolism. *Immunity* **16**, 769–777 (2002). doi:10.1016/S1074-7613(02)00323-0 Medline

6. R. Wang, C. P. Dillon, L. Z. Shi, S. Milasta, R. Carter, D. Finkelstein, L. L. McCormick, P. Fitzgerald, H. Chi, J. Munger, D. R. Green, The transcription factor Myc controls metabolic reprogramming upon T lymphocyte activation. *Immunity* **35**, 871–882 (2011). doi:10.1016/j.immuni.2011.09.021 Medline

7. S. Kouidhi, F. Ben Ayed, A. Benammar Elgaaied, Targeting tumor metabolism: A new challenge to improve immunotherapy. *Front. Immunol.* **9**, 353 (2018). doi:10.3389/fimmu.2018.00353 Medline

8. S. Kouidhi, M. Z. Noman, C. Kieda, A. B. Elgaaied, S. Chouaib, Intrinsic and tumor microenvironment-induced metabolism adaptations of T cells and impact on their differentiation and function. *Front. Immunol.* **7**, 114 (2016). doi:10.3389/fimmu.2016.00114 Medline

9. I. Shevchenko, A. V. Bazhin, Metabolic checkpoints: Novel avenues for immunotherapy of cancer. *Front. Immunol.* **9**, 1816 (2018). doi:10.3389/fimmu.2018.01816 Medline

10. G. C. Prendergast, W. J. Malachowski, A. Mondal, P. Scherle, A. J. Muller, Indoleamine 2,3-dioxygenase and its therapeutic inhibition in cancer. *Int. Rev. Cell Mol. Biol.* **336**, 175–203 (2018). doi:10.1016/bs.ircmb.2017.07.004 Medline

11. E. Zhao, T. Maj, I. Kryczek, W. Li, K. Wu, L. Zhao, S. Wei, J. Crespo, S. Wan, L. Vatan, W. Szeliga, I. Shao, Y. Wang, Y. Liu, S. Varambally, A. M. Chinnaiyan, T. H. Welling, V. Marquez, J. Kotarski, H. Wang, Z. Wang, Y. Zhang, R. Liu, G. Wang, W. Zou, Cancer mediates effector T cell dysfunction by targeting microRNAs and EZH2 via glycolysis restriction. *Nat. Immunol.* **17**, 95–103 (2016). doi:10.1038/ni.3313 Medline

12. D. B. Rivadeneira, G. M. Delgoffe, Antitumor T-cell reconditioning: Improving metabolic fitness for optimal cancer immunotherapy. *Clin. Cancer Res.* **24**, 2473–2481 (2018). doi:10.1158/1078-0432.CCR-17-0894 Medline

13. C. H. Chang, J. Qiu, D. O'Sullivan, M. D. Buck, T. Noguchi, J. D. Curtis, Q. Chen, M. Gindin, M. M. Gubin, G. J. W. van der Windt, E. Tonc, R. D. Schreiber, E. J. Pearce, E. L. Pearce, Metabolic competition in the tumor microenvironment is a driver of cancer progression. *Cell* **162**, 1229–1241 (2015). doi:10.1016/j.cell.2015.08.016 Medline

14. H. Dong, T. N. Bullock, Metabolic influences that regulate dendritic cell function in tumors. *Front. Immunol.* **5**, 24 (2014). doi:10.3389/fimmu.2014.00024 Medline

15. S. M. Davidson, T. Papagiannakopoulos, B. A. Olenchock, J. E. Heyman, M. A. Keibler, A. Luengo, M. R. Bauer, A. K. Jha, J. P. O'Brien, K. A. Pierce, D. Y. Gui, L. B. Sullivan, T. M. Wasylenko, L. Subbaraj, C. R. Chin, G. Stephanopolous, B. T. Mott, T. Jacks, C. B. Clish, M. G. Vander Heiden, Environment impacts the metabolic dependencies of Ras-driven non-small cell lung cancer. *Cell Metab.* **23**, 517–528 (2016). doi:10.1016/j.cmet.2016.01.007 Medline

16. M. Gross, J. Chen, J. Englert, J. Janes, R. Leone, A. MacKinnon, F. Parlati, M. Rodriquez, P. Shwonek, J. Powell, Abstract 2329: Glutaminase inhibition with CB-839 enhances anti-tumor activity of PD-1 and PD-L1 antibodies by overcoming a metabolic checkpoint blocking T cell activation. *Cancer Res.* **76**, 2329 (2016).

17. C. T. Hensley, A. T. Wasti, R. J. DeBerardinis, Glutamine and cancer: Cell biology, physiology, and clinical opportunities. *J. Clin. Invest.* **123**, 3678–3684 (2013). doi:10.1172/JCI69600 Medline

18. L. M. Pinkus, Glutamine binding sites. *Methods Enzymol.* **46**, 414–427 (1977). doi:10.1016/S0076-6879(77)46049-X Medline

19. K. M. Lemberg, J. J. Vornov, R. Rais, B. S. Slusher, We're not "DON" yet: Optimal dosing and prodrug delivery of 6-diazo-5-oxo-L-norleucine. *Mol. Cancer Ther.* **17**, 1824–1832 (2018). doi:10.1158/1535-7163.MCT-17-1148 Medline

20. G. Lynch, N. Kemeny, E. Casper, Phase II evaluation of DON (6-diazo-5-oxo-L-norleucine) in patients with advanced colorectal carcinoma. *Am. J. Clin. Oncol.* **5**, 541–543 (1982). doi:10.1097/00000421-198210000-00014 Medline

21. R. H. Earhart, D. J. Amato, A. Y. Chang, E. C. Borden, M. Shiraki, M. E. Dowd, R. L. Comis, T. E. Davis, T. J. Smith, Phase II trial of 6-diazo-5-oxo-L-norleucine versus aclacinomycin-A in advanced sarcomas and mesotheliomas. *Invest. New Drugs* **8**, 113–119 (1990). doi:10.1007/BF00216936 Medline

22. R. T. Eagan, S. Frytak, W. C. Nichols, E. T. Creagan, J. N. Ingle, Phase II study on DON in patients with previously treated advanced lung cancer. *Cancer Treat. Rep.* **66**, 1665–1666 (1982). Medline

23. G. B. Magill, W. P. L. Myers, H. C. Reilly, R. C. Putnam, J. W. Magill, M. P. Sykes, G. C. Escher, D. A. Karnofsky, J. H. Burchenal, Pharmacological and initial therapeutic observations on 6-diazo-5-oxo-1-norleucine (DON) in human neoplastic disease. *Cancer* **10**, 1138–1150 (1957). doi:10.1002/1097-0142(195711/12)10:6<1138:AID-CNCR2820100608>3.0.CO;2-K Medline

24. S. Krantz, S. Rivers, R. W. Dwight, H. F. Corbus, J. Wolf, I. Green, P. W. Spear, L. T. Imperato, S. Lobe, R. M. Whittington, J. M. Rumball, A. Marquez, C. Cables, A. I. Chernoff, D. K. Misra, R. D. Sullivan, E. Miller, F. S. Dietrich, G. I. Plitman, H. P. Close, S. McCracken, A. S. Glushien, D. L. Rucknagel, C. C. Li, D. Kodlin, A clinical study of the comparative effect of nitrogen mustard and DON in patients with bronchogenic carcinoma, Hodgkin's disease, lymphosarcoma, and melanoma. *J. Natl. Cancer Inst.* **22**, 433–439 (1959). doi:10.1093/jnci/22.2.433 Medline

25. R. Rais, A. Jančařík, L. Tenora, M. Nedelcovych, J. Alt, J. Englert, C. Rojas, A. Le, A. Elgogary, J. Tan, L. Monincová, K. Pate, R. Adams, D. Ferraris, J. Powell, P. Majer, B. S. Slusher, Discovery of 6-diazo-5-oxo-l-norleucine (DON) prodrugs with enhanced CSF delivery in monkeys: A potential treatment for glioblastoma. *J. Med. Chem.* **59**, 8621–8633 (2016). doi:10.1021/acs.jmedchem.6b01069 Medline

26. J. Fu, E. Pacyniak, M. G. D. Leed, M. P. Sadgrove, L. Marson, M. Jay, Interspecies differences in the metabolism of a multiester prodrug by carboxylesterases. *J. Pharm. Sci.* **105**, 989–995 (2016). doi:10.1002/jps.24632 Medline

27. J. Van Gelder, M. Shafiee, E. De Clercq, F. Penninckx, G. Van den Mooter, R. Kinget, P. Augustijns, Species-dependent and site-specific intestinal metabolism of ester prodrugs. *Int. J. Pharm.* **205**, 93–100 (2000). doi:10.1016/S0378-5173(00)00507-X Medline

28. JHU083 is referred to as “compound 3” in (*19*) and “compound 4a” in (*25*).

29. X. Zhu, M. T. Nedelcovych, A. G. Thomas, Y. Hasegawa, A. Moreno-Megui, W. Coomer, V. Vohra, A. Saito, G. Perez, Y. Wu, J. Alt, E. Prchalova, L. Tenora, P. Majer, R. Rais, C. Rojas, B. S. Slusher, A. Kamiya, JHU-083 selectively blocks glutaminase activity in brain CD11b$^+$ cells and prevents depression-associated behaviors induced by chronic social defeat stress. *Neuropsychopharmacology* **44**, 683–694 (2019). doi:10.1038/s41386-018-0177-7 Medline

30. M. T. Nedelcovych, B.-H. Kim, X. Zhu, L. E. Lovell, A. A. Manning, J. Kelschenbach, E. Hadas, W. Chao, E. Prchalová, R. P. Dash, Y. Wu, J. Alt, A. G. Thomas, R. Rais, A. Kamiya, D. J. Volsky, B. S. Slusher, Glutamine antagonist JHU083 normalizes aberrant glutamate production and cognitive deficits in the EcoHIV murine model of HIV-associated neurocognitive disorders. *J. Neuroimmune Pharmacol.* **14**, 391–400 (2019). doi:10.1007/s11481-019-09859-w Medline

31. B. Murter, X. Pan, E. Ophir, Z. Alteber, M. Azulay, R. Sen, O. Levy, L. Dassa, I. Vaknin, T. Fridman-Kfir, R. Salomon, A. Ravet, A. Tam, D. Levin, Y. Vaknin, E. Tatirovsky, A. Machlenkin, D. Pardoll, S. Ganguly, Mouse PVRIG Has CD8$^+$ T cell-specific coinhibitory functions and dampens antitumor immunity. *Cancer Immunol. Res.* **7**, 244–256 (2019). doi:10.1158/2326-6066.CIR-18-0460 Medline

32. B. L. Horton, J. B. Williams, A. Cabanov, S. Spranger, T. F. Gajewski, Intratumoral CD8$^+$ T-cell apoptosis is a major component of T-cell dysfunction and impedes antitumor immunity. *Cancer Immunol. Res.* **6**, 14–24 (2018). doi:10.1158/2326-6066.CIR-17-0249 Medline

33. D. A. Chisolm, D. Savic, A. J. Moore, A. Ballesteros-Tato, B. León, D. K. Crossman, C. Murre, R. M. Myers, A. S. Weinmann, CCCTC-binding factor translates interleukin 2- and α-ketoglutarate-sensitive metabolic changes in T cells into context-dependent gene programs. *Immunity* **47**, 251–267.e7 (2017). doi:10.1016/j.immuni.2017.07.015 Medline

34. P. A. Tyrakis, A. Palazon, D. Macias, K. L. Lee, A. T. Phan, P. Veliça, J. You, G. S. Chia, J. Sim, A. Doedens, A. Abelanet, C. E. Evans, J. R. Griffiths, L. Poellinger, A. W. Goldrath, R. S. Johnson, *S*-2-hydroxyglutarate regulates CD8$^+$ T-lymphocyte fate. *Nature* **540**, 236–241 (2016). doi:10.1038/nature20165 Medline

35. G. J. van der Windt, B. Everts, C.-H. Chang, J. D. Curtis, T. C. Freitas, E. Amiel, E. J. Pearce, E. L. Pearce, Mitochondrial respiratory capacity is a critical regulator of CD8$^+$ T cell

memory development. *Immunity* **36**, 68–78 (2012). doi:10.1016/j.immuni.2011.12.007 Medline

36. M. L. Balmer, E. H. Ma, G. R. Bantug, J. Grählert, S. Pfister, T. Glatter, A. Jauch, S. Dimeloe, E. Slack, P. Dehio, M. A. Krzyzaniak, C. G. King, A.-V. Burgener, M. Fischer, L. Develioglu, R. Belle, M. Recher, W. V. Bonilla, A. J. Macpherson, S. Hapfelmeier, R. G. Jones, C. Hess, Memory $CD8^+$ T cells require increased concentrations of acetate induced by stress for optimal function. *Immunity* **44**, 1312–1324 (2016). doi:10.1016/j.immuni.2016.03.016 Medline

37. J. Qiu, M. Villa, D. E. Sanin, M. D. Buck, D. O'Sullivan, R. Ching, M. Matsushita, K. M. Grzes, F. Winkler, C.-H. Chang, J. D. Curtis, R. L. Kyle, N. Van Teijlingen Bakker, M. Corrado, F. Haessler, F. Alfei, J. Edwards-Hicks, L. B. Maggi Jr., D. Zehn, T. Egawa, B. Bengsch, R. I. Klein Geltink, T. Jenuwein, E. J. Pearce, E. L. Pearce, Acetate promotes T cell effector function during glucose restriction. *Cell Reports* **27**, 2063–2074.e5 (2019). doi:10.1016/j.celrep.2019.04.022 Medline

38. S. K. Vodnala, R. Eil, R. J. Kishton, M. Sukumar, T. N. Yamamoto, N.-H. Ha, P.-H. Lee, M. Shin, S. J. Patel, Z. Yu, D. C. Palmer, M. J. Kruhlak, X. Liu, J. W. Locasale, J. Huang, R. Roychoudhuri, T. Finkel, C. A. Klebanoff, N. P. Restifo, T cell stemness and dysfunction in tumors are triggered by a common mechanism. *Science* **363**, eaau0135 (2019). doi:10.1126/science.aau0135 Medline

39. S. Jitrapakdee, A. Vidal-Puig, J. C. Wallace, Anaplerotic roles of pyruvate carboxylase in mammalian tissues. *Cell. Mol. Life Sci.* **63**, 843–854 (2006). doi:10.1007/s00018-005-5410-y Medline

40. T. Cheng, J. Sudderth, C. Yang, A. R. Mullen, E. S. Jin, J. M. Matés, R. J. DeBerardinis, Pyruvate carboxylase is required for glutamine-independent growth of tumor cells. *Proc. Natl. Acad. Sci. U.S.A.* **108**, 8674–8679 (2011). doi:10.1073/pnas.1016627108 Medline

41. K. Sellers, M. P. Fox, M. Bousamra II, S. P. Slone, R. M. Higashi, D. M. Miller, Y. Wang, J. Yan, M. O. Yuneva, R. Deshpande, A. N. Lane, T. W.-M. Fan, Pyruvate carboxylase is critical for non-small-cell lung cancer proliferation. *J. Clin. Invest.* **125**, 687–698 (2015). doi:10.1172/JCI72873 Medline

42. M. St. Maurice, L. Reinhardt, K. H. Surinya, P. V. Attwood, J. C. Wallace, W. W. Cleland, I. Rayment, Domain architecture of pyruvate carboxylase, a biotin-dependent multifunctional enzyme. *Science* **317**, 1076–1079 (2007). doi:10.1126/science.1144504 Medline

43. M. F. Utter, D. B. Keech, Pyruvate carboxylase. I. Nature of the reaction. *J. Biol. Chem.* **238**, 2603–2608 (1963). Medline

44. F. R. Dejure, N. Royla, S. Herold, J. Kalb, S. Walz, C. P. Ade, G. Mastrobuoni, J. T. Vanselow, A. Schlosser, E. Wolf, S. Kempa, M. Eilers, The *MYC* mRNA 3′-UTR couples RNA polymerase II function to glutamine and ribonucleotide levels. *EMBO J.* **36**, 1854–1868 (2017). doi:10.15252/embj.201796662 Medline

45. B. Faubert, G. Boily, S. Izreig, T. Griss, B. Samborska, Z. Dong, F. Dupuy, C. Chambers, B. J. Fuerth, B. Viollet, O. A. Mamer, D. Avizonis, R. J. DeBerardinis, P. M. Siegel, R. G. Jones, AMPK is a negative regulator of the Warburg effect and suppresses tumor growth in vivo. *Cell Metab.* **17**, 113–124 (2013). doi:10.1016/j.cmet.2012.12.001 Medline

46. H. M. Haikala, J. M. Anttila, J. Klefström, MYC and AMPK—Save energy or die! *Front. Cell Dev. Biol.* **5**, 38 (2017). doi:10.3389/fcell.2017.00038 Medline

47. J. W. Kim, C. V. Dang, Cancer's molecular sweet tooth and the Warburg effect. *Cancer Res.* **66**, 8927–8930 (2006). doi:10.1158/0008-5472.CAN-06-1501 Medline

48. A. B. Kohan, I. Talukdar, C. M. Walsh, L. M. Salati, A role for AMPK in the inhibition of glucose-6-phosphate dehydrogenase by polyunsaturated fatty acids. *Biochem. Biophys. Res. Commun.* **388**, 117–121 (2009). doi:10.1016/j.bbrc.2009.07.130 Medline

49. Z. E. Stine, Z. E. Walton, B. J. Altman, A. L. Hsieh, C. V. Dang, MYC, metabolism, and cancer. *Cancer Discov.* **5**, 1024–1039 (2015). doi:10.1158/2159-8290.CD-15-0507 Medline

50. O. Warburg, K. Gawehn, A. W. Geissler, Stoffwechsel der weissen Blutzellen. *Z. Naturforsch. B* **13**, 515–516 (1958). doi:10.1515/znb-1958-0806 Medline

51. A. Bakker, Einige Übereinstimmungen im Stoffwechsel der Carcinomzellen und Exsudatleukocyten. *Klin. Wochenschr.* **6**, 252–254 (1927). doi:10.1007/BF01710710

52. V. A. Gerriets, J. C. Rathmell, Metabolic pathways in T cell fate and function. *Trends Immunol.* **33**, 168–173 (2012). doi:10.1016/j.it.2012.01.010 Medline

53. N. J. MacIver, R. D. Michalek, J. C. Rathmell, Metabolic regulation of T lymphocytes. *Annu. Rev. Immunol.* **31**, 259–283 (2013). doi:10.1146/annurev-immunol-032712-095956 Medline

54. E. L. Pearce, M. C. Poffenberger, C. H. Chang, R. G. Jones, Fueling immunity: Insights into metabolism and lymphocyte function. *Science* **342**, 1242454 (2013). doi:10.1126/science.1242454 Medline

55. P. J. Siska, K. E. Beckermann, F. M. Mason, G. Andrejeva, A. R. Greenplate, A. B. Sendor, Y. J. Chiang, A. L. Corona, L. F. Gemta, B. G. Vincent, R. C. Wang, B. Kim, J. Hong, C. L. Chen, T. N. Bullock, J. M. Irish, W. K. Rathmell, J. C. Rathmell, Mitochondrial dysregulation and glycolytic insufficiency functionally impair CD8 T cells infiltrating human renal cell carcinoma. *JCI Insight* **2**, e93411 (2017). doi:10.1172/jci.insight.93411 Medline

56. M. V. Liberti, J. W. Locasale, The Warburg effect: How does it benefit cancer cells? *Trends Biochem. Sci.* **41**, 211–218 (2016). doi:10.1016/j.tibs.2015.12.001 Medline